06 Apr 1995, 10:30 am - 12:30 pm

Numerical Simulations of Soil Liquefaction using Stochastic Input Parameters

R. Popescu
Princeton University, Princeton, NJ

J. H. Prevost
Princeton University, Princeton, NJ

E. H. Vanmarcke
Princeton University, Princeton, NJ

Proceedings: Third International Conference on Recent Advances in Geotechnical Earthquake Engineering and Soil Dynamics, April 2–7, 1995, Volume I, St. Louis, Missouri

Numerical Simulations of Soil Liquefaction using Stochastic Input Parameters

Paper No. 3.35

R. Popescu, J.H. Prevost and E.H. Vanmarcke
Department of Civil Engineering and Operations Research, Princeton University, Princeton, NJ

SYNOPSIS The influence of spatial variability of soil properties on the results of numerical simulations of dynamically induced pore water pressure is addressed. Random media of N_{SPT} values are generated based on in situ test results. The soil geomechanical properties are evaluated at each location, function of the N_{SPT} values, and finite element simulations of the behaviour of a horizontally layered soil subjected to seismic loading are performed. The influence of : (1) assumed distribution of the underlying random variable, (2) scale of fluctuation, and (3) finite element mesh size are discussed in terms of predicted liquefaction index and excess pore pressure build–up.

1. INTRODUCTION

Soil properties are known to exhibit spatial variability in most natural deposits, even within so called "homogeneous" layers. However, in most numerical simulations, soil materials are considered as having constant (deterministic) properties within certain regions (e.g. soil layers). The constitutive model parameters are evaluated on the basis of in situ and/or laboratory soil test results, usually by averaging the outcomes of several tests.

The paper emphasizes the effects of random spatial variability of soil properties on the results of numerical simuations of dynamically induced pore water pressures. Using a (relatively scarce) set of in situ data – Standard Penetration Test results (N_{SPT}) for saturated sandy soils measured at Akita Harbour [4] – first the statistics of N_{SPT} spatial distribution are evaluated, and then a method to generate a 2D random field, based on covariances of local averages, [17, 18] is emploied to obtain several possible 2D distributions of the N_{SPT} values within the analysis region. Numerical simulations are performed using the finite element code DYNAFLOW [10]. The constitutive model parameters are evaluated function of the N_{SPT} values generated at finite element locations, using correlation formulae and liquefaction strength evaluations. Comparisons between the results of stochastic input parameter computations vs. those of the corresponding deterministic analysis point out to the importance of spatial variability of soil properties.

2. FIELD DATA ANALYSIS

To illustrate the analysis method, a site in Akita Harbour (Japan) has been selected. The region was hit by the Nihonkai–Chubu Earthquake (May, 1983, Magnitude 7.7) and extensive damage due to soil liquefaction was reported. The specific location selected for the present analysis is Ohama No. 1 Wharf, where three borings with consistent SPT measurements are available [4]. The soil consists of quaternary deposits of medium to dense sands and did not liquefy during the earthquake. Two layers with slightly different geomechanical properties are identified: a medium grain size sand ($D_{50} \approx 0.6$mm), underlied by a fine sand layer, with $D_{50} \approx 0.15$mm.

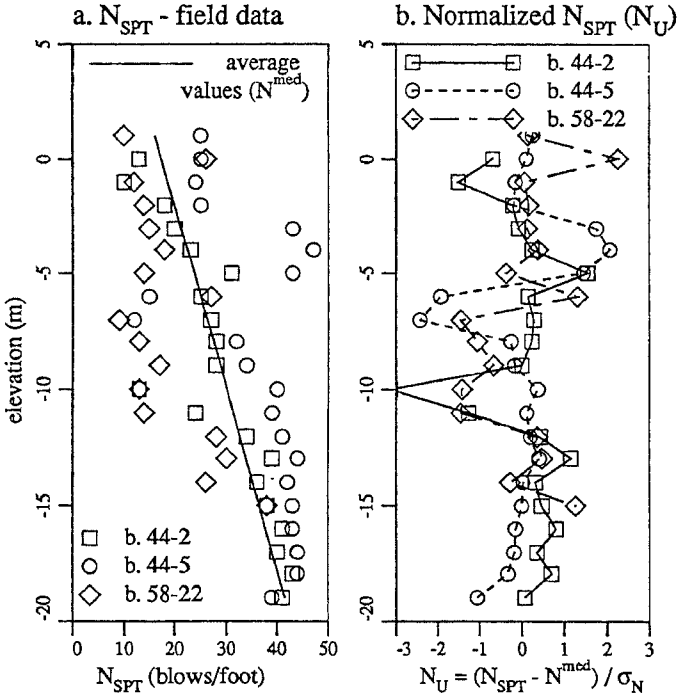

Fig. 1. N_{SPT} data from Akita Harbour – Ohama No. 1 Wharf (from ref. [4]).

2.1. Normalisation of field data

The SPT results (Figure 1.a) are reported at 1m vertical distance, for up to 20m below the water table (water table is at +1m in Figure 1). The field data are clearly

non–homogeneous in the mean, nor in standard deviation. To obtain a homogeneous 2D random medium, more suitable for random field analysis procedures, the field data are normalized as shown hereafter.

A unique linear expression for the mean is computed for all the borings using the least square method:

$$N^{med}(y) = 17.4 - 1.27\, y \qquad (1)$$

with y – elevation in meters (negative with depth). The variance at each elevation, $\sigma_N(y)$, is computed using the values of 7 neighboring measurements from each boring, and the N_{SPT} data at each boring are normalised, obtaining a zero mean, unit standard deviation series, plotted in Figure 1,b:

$$N_U(y) = \left[N_{SPT}(y) - N^{med}(y)\right] / \sigma_N(y) \qquad (2)$$

2.2. Distribution of the underlying random variable

As inferred from the results of the numerical example (§4.3.), the computational results are dependent on the assumed distribution of the underlying random variable of the random medium (N_U). Two possible distributions are considered in the study: Gaussian and Lognormal. Their valability for modeling the random media of normalized N_{SPT} values is checked by quantile–quantile plots. The q–q plots shown in Figure 2 validate the Gaussian distribution for the N_{SPT} values measured at that particular site.

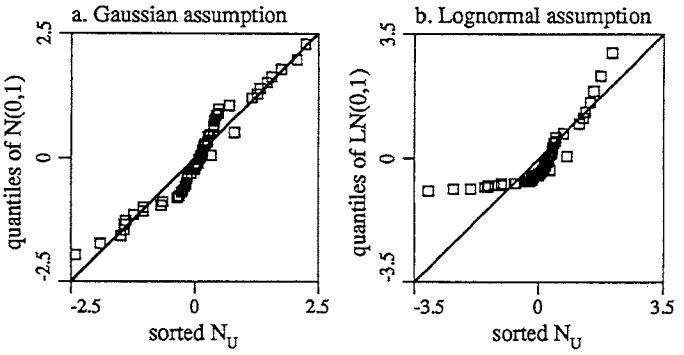

Fig. 2. Quantile–quantile plots for validation of distribution assumption.

2.3. Evaluation of the scales of fluctuation

To account for the differences induced by geological stratification, the correlation structure for the random medium representing soil properties is assumed separable. For the 2D case, this means that the variance function is the product of two 1D variance functions [17] depending respectively on horizontal and vertical scales of fluctuation. A triangular correlation structure in vertical direction and a Gaussian shaped correlation structure in horizontal direction are adopted for this study.

The **vertical** scale of fluctuation is evaluated in two ways [17]:

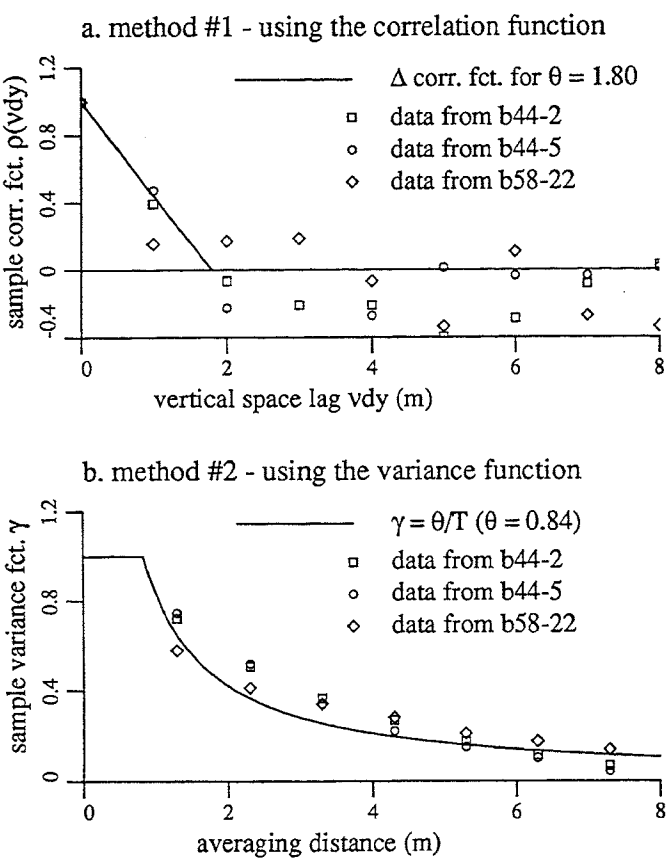

Fig. 3. Evaluation of the fluctuation scale in vertical direction (θ_y) from field data.

1. Using the correlation function. For each boring, the sample correlation function can be computed using a discretized formulation of the general expression (see e.g. [17]) which, for a discrete stationary random process x_k with zero mean and unit standard deviation, simplifies to:

$$\rho(\nu dy) = \frac{1}{n-\nu} \sum_{k=1}^{n-\nu} x_k x_{k+\nu} \qquad (3)$$

with: νdy – the space lag, dy – vertical distance between measurements, and n – number of measurements in each boring. The scale of fluctuation can be then found by fitting the results for a specific correlation structure. For the triangular correlation structure, the resulted value is about 1.8m (Figure 3.a).

2. Using the variance function. The sample variance function is computed for each boring function of the number of averaged neighboring measurements – ν:

$$\gamma[(\nu-1)dy + a] = \frac{\sigma_\nu}{\sigma} \qquad (4)$$

with: σ_ν – standard deviation of locally averaged values, $\sigma = 1.0$, and $a \approx 30$cm – to account for the measurement method, i.e. the fact that N_{SPT} is the number of blows necessary to penetrate *1 ft.* into the ground. Accounting for the assymptotic expression of the variance function for relatively large values of the averaging

interval T [17]: $\gamma(T) \approx \frac{\theta}{T}$, for $T \gg \theta$, the scale of fluctuation $\theta_y = 0.84$m is found using the least square error method, for values $T = 5 \ldots 8$m (Figure 3.b).

Very scarce data is available to evaluate the **horizontal** scale of fluctuation. The evaluation method is based on the computation of sample correlation coeficient between measurement results from adjacent borings. Assuming a gaussian correlation structure in the horizontal direction, the horizontal scale of fluctuation results $\theta_x \approx 40$m, for a 35m distance between adjacent borings.

Remark: The available data is clearly insufficient for the evaluation of fluctuation scales (too little information on horizontal correlation and sampling interval close to the correlation length in both horizontal and vertical directions). However, the computed values are within the range of other results from previous similar studies: Vanmarcke [16] computed a vertical correlation length $\theta_y = 1.2$ m for the vertical distribution of cone penetration test results; Fenton [2] estimated scales of fluctuation $\theta_x = 40$ m and $\theta_y = 1$m for the soil properties at the Wildlife Liquefaction Site.

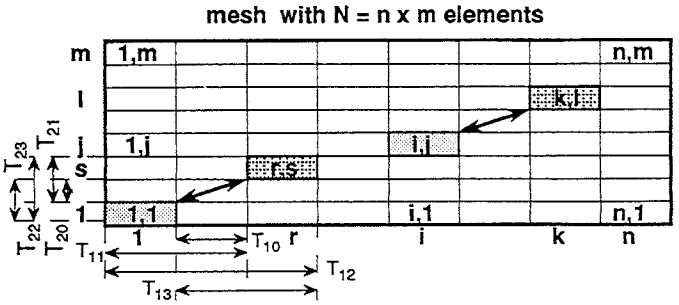

A. COVARIANCE MATRIX $\mathbf{B}[N \times N]$, $N = n \times m$

1. First line: $\mathbf{B}[(1,1);(r,s)]$, $r = 1,n \quad s = 1,m$:

$$\mathbf{B}[(1,1);(r,s)] = \frac{\sigma^2}{4\mathrm{dx}^2\mathrm{dy}^2} \sum_{k=0}^{3}\sum_{l=0}^{3} (-1)^{k+l} \Delta(T_{1k}, T_{2l})$$

2. Subsequent lines:

$$\mathbf{B}[(i,j);(k,l)] = \mathbf{B}[(1,1);(r,s)]$$

B. RANDOM FIELD GENERATION

1. Given $\mathbf{B}[N \times N]$, solve the eigenvalue problem:

$$[\mathbf{B} - \lambda_k \mathbf{I}]\, \mathbf{X}_k = 0 \;\Rightarrow\; \begin{cases} \lambda_k - \text{eigenvalues} \\ \mathbf{X}_k - \text{eigenvectors} \end{cases}$$

$$\text{or} \qquad \mathbf{D} = \begin{pmatrix} \lambda_1 & \cdots & 0 \\ \vdots & \ddots & \vdots \\ 0 & \cdots & \lambda_N \end{pmatrix} \qquad \mathbf{X} = [\mathbf{X}_1, \cdots, \mathbf{X}_N]$$

and $\mathbf{D} = \mathbf{X}\mathbf{B}\mathbf{X}^T$ – covariance matrix of a R.F. $\mathbf{Z}$, with:
- $\mathbf{Z}_1, \cdots, \mathbf{Z}_N$ – uncorrelated random variables;
- $\lambda_1, \cdots, \lambda_N$ – respective variances.

2. **Given D and X, generate Z** (N independent random variables, with variances $\sigma_{Zk} = \lambda_k$), and: $\mathbf{N_U} = \mathbf{X}^T \times \mathbf{Z}$ is the required R. F. corresponding to the covariance matrix $\mathbf{B}$

Fig. 4. Algorithm for 2D Random Field generation [17].

3. 2D RANDOM FIELD GENERATION

A soil region below the water table, 100m in horizontal direction × 20m in depth, is included in the stochastic input analysis domain. The material properties for the sand situated above the water table are assumed deterministic. For given statistics ($m = 0$, $\sigma = 1$, θ_x and θ_y) and for a uniform rectangular finite element mesh, a 2D random field with separable correlation structure is generated. First, the covariance matrix is computed using the expression of covariance of local averages [17], and then the random field is generated based on the positive definiteness of the covariance matrix. The algorithm is presented in the flowchart in Figure 4.

Remarks:

1. For the case at hand, the adopted variance function is (see §2.3.): $\gamma(\nu_x, \nu_y) = \gamma_x(\nu_x) \times \gamma_y(\nu_y)$. The expressions of γ_x and γ_y, for Gaussian and triangular shaped correlation structures, respectively, are given in ref. [17].

2. The covariance matrix computation for a rectangular mesh and a quadrant symmetric random field is reduced to the computation of the first line (Figure 4).

3. The generation of more random fields with the same statistics can be sped–up by storing the eigenvalues $\mathbf{D}$ and eigenvectors $\mathbf{X}$ and performing only the last part of the algorithm.

Several 2D zero mean and unit standard deviation Gaussian random fields for various mesh sizes have been generated using the scales of fluctuation evaluated at §2.3. The computation method is checked by comparing sample correlation and variance functions of vertical

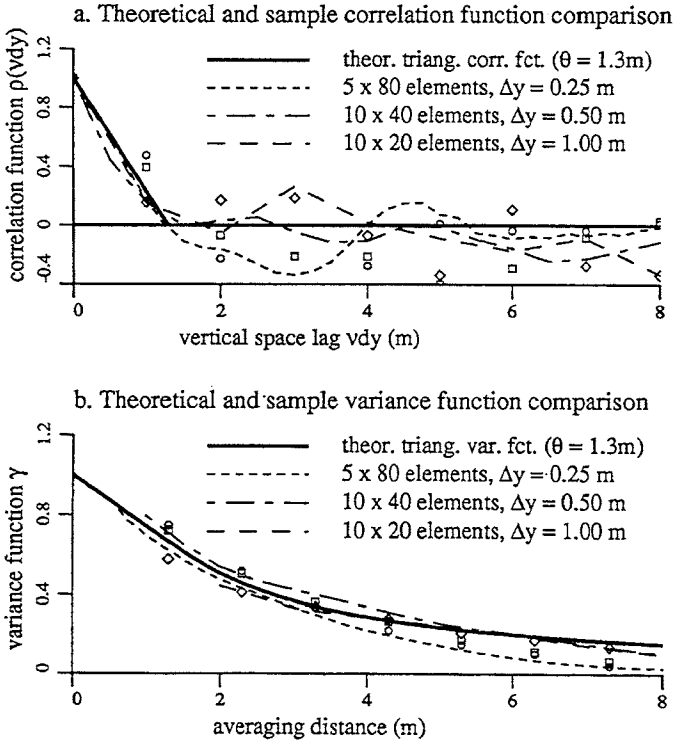

Fig. 5. Comparison between generated (dashed lines) and theoretical (continuous lines) correlation and variance functions, evaluated for the vertical direction. Results from field data are represented with markers.

sections picked from the generated random fields (dotted lines) with the theoretical values (continuous lines) in Figure 5. The values computed from field data are represented with markers in the same figure.

Zero mean, unit standard deviation values generated at the locations of finite element centroids ($N_U(x,y)$) are transformed to total N_{SPT} values, using:

$$N_{SPT}(x,y) = N_U(x,y) \times \sigma_{\mathrm{d}x\mathrm{d}y}(y) + N^{med}(y) \qquad (5)$$

where $\sigma_{\mathrm{d}x\mathrm{d}y}(y)$ is the standard deviation of the resulted random field, $N_{SPT}(x,y)$, variable with depth – as shown in §2.1., and accounting for the local averaging over finite elements:

$$\sigma_{\mathrm{d}x\mathrm{d}y}(y) = \frac{\sigma_N(y)}{\gamma_y(0.3\mathrm{m})} \cdot \gamma_y(\mathrm{d}x) \cdot \gamma_z(\mathrm{d}y) \qquad (6)$$

In eqn. (6), the reduction of N_{SPT} test result standard deviation, $\sigma_N(y)$, due to local averaging imposed by the testing method, is accounted for.

4. FINITE ELEMENT DYNAMIC ANALYSES

The computer code DYNAFLOW [10] is a finite element program for nonlinear seismic site response analysis. Dry and saturated deposits can be analysed. The solid and fluid coupled field equations [1] and constitutive equations [11] are general and applicable to multi-dimensional situations. The multi–yield surface plasticity model used for numerical simulations is a kinematic hardening model based on a relatively simple plasticity theory [11] and is applicable to both cohesive and cohesionless soils.

4.1. Constitutive model parameter evaluation

All the required constitutive model parameters can be derived from the results of conventional laboratory (e.g. "triaxial", "simple shear") and in–situ (e.g. "wave velocity", "standard penetration") soil tests [12, 8].

Table 1. Multi–yield plasticity model constitutive parameters

Constitutive parameter	Symbol	Type
Mass density - solid	ρ_s	State parameters
Porosity	n^w	
Permeability	k	
Low strain moduli	G_0 , B_0	Low strain elastic parameters
Ref. mean effective stress	p_0	
Power exponent	n	
Friction angle at failure	ϕ	Yield and failure parameters
Stress–strain curve coeff. [3]	α	
Maximum deviatoric strain	ε_{dev}^{max}	
Dilation angle	ϕ	Dilation parameters
Dilation parameter (cyclic)	X_{pp}	

The required constitutive soil parameters for the multi-yield plasticity model, are summarized in Table 1. In this study, some of these parameters were considered constant for each soil layer, other (namely: porosity, permeability, low strain moduli, friction angle, dilation angle and dilation parameter) variable with the Standard Penetration Resistance of the soil. The functional expressions relating soil parameter values and Standard Penetration Resistance are derived from correlation formulae reported in the literature (e.g. ref. [7] for the low strain shear modulus). Some of the soil parameters are evaluated from correlations with relative density (e.g. ref. [6] for friction angle at failure and [5] for dilation angle), which in turn, is related to the normalized Standard Penetration Resistance $N_{1(60)}$ (e.g. ref. [15]). The dilation parameter (Xpp), which controls the amount of plastic dilation and, consequently of pore pressure build–up, is dependent on both N_{SPT} and confining stress. The details of Xpp evaluation from liquefaction strength analysis, using element tests and the relationship between stress ratio causing liquefaction and normalised N_{SPT} values [13] are presented in refs. [8, 9].

4.2. Numerical simulation set–up

A zone of 100m in horizontal direction and 23m in elevation (3m above the water table) is analysed. Finite Element computations are performed to simulate the behaviour of saturated soil subjected to seismic excitation. A period of 15 sec. of the E–W accelerogram recorded at the site during the Nihonkai–Chubu Earthkuaqe is selected as input motion (Figure 6). The recorded amplitudes are doubled to obtain a more significant pore

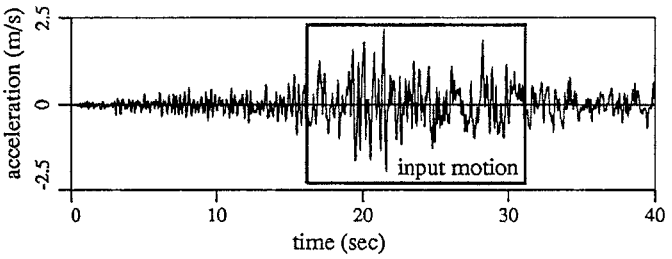

Fig. 6. Acceleration record at Akita Harbour (E–W direction) during the 1983 Nihonkai–Chubu Earthquake.

water pressure build–up. The input motion is applied at the base nodes of the mesh, in horizontal direction.

The **deterministic input** computations are performed using a mesh represented by a column of 20 two phase medium elements (for the saturated material) and 1 one phase medium material (for the dry soil). The material properties at each elevation are evaluated using the average values $N^{med}(y)$ – eqn. (1).

Most of the **stochastic input** computations are performed on a mesh with 10 (in horizontal direction) × 20 (in vertical direction) finite elements in the saturated material zone. The mesh size influence is checked using a finer (20 × 40 elements) and a coarser (5×10 elements) mesh. To account for the inherent variability in computational results, several numerical simulations are performed using random fields with similar

characteristics, generated on a mesh of 10 × 20 finite elements: 7 Gaussian and 7 Lognormal random fields generated using the best estimates for the fluctuation scales (§2.3), and 5 Gaussian random fields, with larger scales of fluctuation, $\theta_x = 100$m and $\theta_y = 5$m.

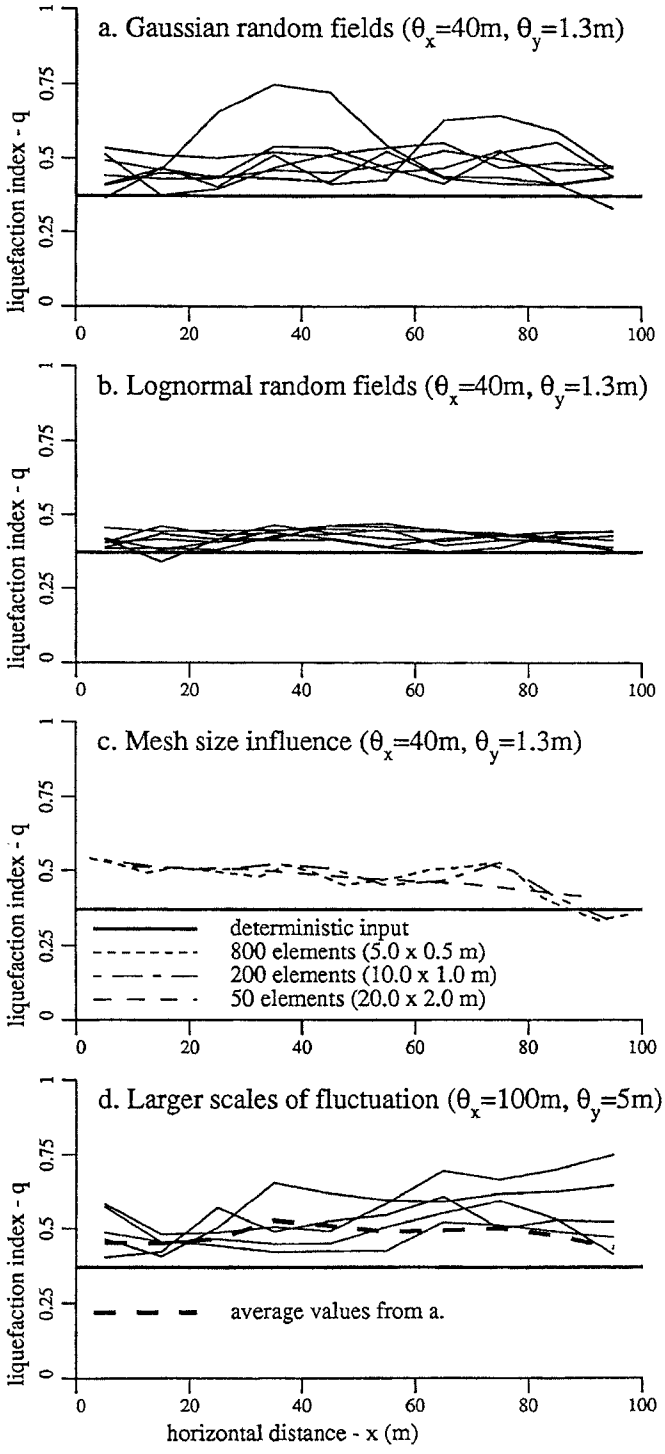

Fig. 7. Comparisons between finite element computational results in terms of liquefaction index. Deterministic input parameter results are shown with solid horizontal lines.

4.3. Numerical computation results

The resulted excess pore pressures are compared in Figure 7 in terms of the Liquefaction index [14], computed for vertical sections (in eqn. (7), vertical section "i" has abscise "x", and horizontal layer "j" of finite elements has elevation "y"):

$$Q(x) = \frac{1}{H}\int_0^H \frac{u(x,y)}{\sigma_{v0}(x,y)}dy \quad \text{or}$$
$$Q_i = \frac{1}{m}\sum_{j=1}^{m}\frac{u_{ij}}{\sigma_{v0,ij}} \qquad i = 1,n \tag{7}$$

with: $H = 20$m – thickness of the submerged zone; n, m – number of elements in horizontal and vertical directions, respectively; $u(x,y)$ or u_{ij} – computed excess pore pressure in the finite element i,j; $\sigma_{v0}(x,y)$ or $\sigma_{v0,ij}$ – initial effective vertical stress in the finite element i,j.

From the results presented in Figure 7, it can be inferred that:

1. The liquefaction indices resulted from stochastic input computations have larger values than those computed with deterministic input (solid horizontal lines in Figure 7) for all the cases analysed.
2. The choice of distribution function for the underlying random variable has significant influence on the computation results: overall liquefaction index values are about 25% larger in the case of Gaussian random fields than for Lognormal random fields (Figure 7.a,b).
3. The computed liquefaction indices seem to be quite insensitive to the mesh size, as long as finite element dimensions are smaller than the respective scales of fluctuation (e.g. $dy \leq 1$ m, as compared to $\theta_y = 1.3$ m) – Figure 7.c. It is to be noticed that the study on mesh size influence is performed using the same random field for all three cases. The N_{SPT} values obtained for the finer mesh (20×40 elements) are locally averaged to accomodate the other two meshes.
4. By using larger scales of fluctuation, the resulted excess pore pressures tend to increase (by about 10%, on average, for the cases studied here) – Figure 7.d.

5. CONCLUSIONS

The study has a series of limitations, mainly imposed by the scarcity of available field data, on the one hand, and by the computational effort required by fully nonlinear dynamic finite element analyses, on the other hand: (1) the assumed distribution function of the underlying random variable should better accomodate the real distribution of in situ measured N_{SPT} values, which have a limited domain of variation; (2) some of the constitutive model parameters are considered deterministic; (3) perfect correlation is assumed among stochastic soil parameters, since they all are evaluate in terms of a single random variable – N_{SPT}; (4) the case study only refers to a soil with relatively high liquefaction resistance; behaviour of looser saturated sands, involving

more nonlinearity when subjected to dynamic loading, should also be analysed. With the reserve of those limitations, the folowing conclusions are stated:

1. A procedure to generate a 2D random field with separable correlation structure is presented on the basis of a real site analysis.

2. The multi–yield surface model constitutive parameters are evaluated as functions of the N_{SPT} value and confining stress (depth).

3. Comparisons between the results of deterministic and stochastic input Finite Element calculations show that larger overall pore pressure build–up is obtained by using stochastic than deterministic input parameters.

4. The choice of distribution function for the underlying random variables has significant influence on the computational results.

5. As long as the finite element dimensions are smaller than the scales of fluctuation, the overall computation results are almost insensitive to the mesh size.

6. For the cases analysed, the results show that variation of fluctuation scales has little influence on the excess pore pressure magnitude; however, to arrive at a definite conclusion, a larger palette of fluctuation scale values should be considered.

ACKNOWLEDGEMENTS

The work reported in this study was supported in part by a grant from Kajima Corporation, Japan to Princeton University. This support is most gratefully acknowledged.

References

[1] M.A. Biot. Mechanics of deformation and acoustic propagation in porous media. *J. Appl. Phys.*, 33(4):1482–1498, 1962.

[2] G.A. Fenton. *Simulation and Analysis of Random Fields.* PhD thesis, Princeton Univ., 1990.

[3] H. Hayashi, M. Honda, and T. Yamada. Modeling of nonlinear stress strain relations of sands for dynamic response analysis. In *Proc. 10th World Conf. on Earthquake Eng., Madrid, Spain.* Balkema, Rotterdam, 1992. Invited paper.

[4] S. Iai. A strain space multiple mechanism model for cyclic behaviour of sand and its application. Technical report, EERG, Port and Harbour Res. Inst., Japan, 1991.

[5] R.M. Koerner. Effect of particle characteristics on soil strength. *J. Soil Mech. Found. Div., ASCE*, 96(SM4):1221–1234, 1970.

[6] Naval Fac. Eng. Command, Alexandria. *Soil Mechanics (DM 7.1)*, 1982.

[7] Y. Ohsaki and R. Iwasaki. On dynamic shear moduli and Poisson's ratio of soil deposits. *Soils and Foundations*, 13(4):61–73, 1973.

[8] R. Popescu and J.H. Prevost. Centrifuge validation of a numerical model for dynamic soil liquefaction. *Soil Dynamics and Earthquake Eng.*, 12(2):73–90, 1993.

[9] R. Popescu and J.H. Prevost. Numerical Class "A" predictions for Models No. 1, 2, 3, 4a, 4b, 6, 7, 11 and 12. In *Proc. Int. Conf. on Verif. Numerical Proc. for the Analysis of Soil Liq. Problems*, volume 1, pages 1105–1207. Balkema, Rotterdam, 1993.

[10] J.H. Prevost. DYNAFLOW: A nonlinear transient finite element analysis program. Dept. of Civil Eng. and Op. Research, Princeton University, 1981. Last update 1993.

[11] J.H. Prevost. A simple plasticity theory for frictional cohesionless soils. *Soil Dynamics and Earthquake Eng.*, 4:9–17, 1985.

[12] J.H. Prevost. Nonlinear dynamic response analysis of soil and soil–structure interacting systems. In *Proc. Seminar Soil Dyn. Geotech. Earthq. Eng., Lisboa, Portugal*, pages 49–126. Balkema, Rotterdam, 1993.

[13] H.B. Seed, I.M. Idriss, and I. Arango. Evaluation of liquefaction potential using field performance data. *J. Geotech. Eng., ASCE*, 109(3):458–482, 1983.

[14] M. Shinozuka and K. Ohtomo. Spatial severity of liquefaction. In *Proc. 2nd U.S.–Japan Workshop on Liquefaction, Large Ground Deformation and their Effects on Lifelines*, 1989.

[15] A.W. Skempton. Standard penetration test procedures and the effects in sands of overburden pressure, relative density, particle size, ageing and overconsolidation. *Geotechnique*, 36(3):425–447, 1986.

[16] E.H. Vanmarcke. Probabilistic modeling of soil profiles. *Journ. Geotech. Eng. Div.*, 103(GT11):1227–1246, 1977.

[17] E.H. Vanmarcke. *Random Fields: Analysis and Synthesis.* The MIT Press, 1984.

[18] E.H. Vanmarcke. Stochastic finite elements and experimental measurements. In *Int. Conf. on Comp. Meth. Exp. Measur., Capri, Italy*, pages 137–155. Springer–Verlag, 1989.